Electronic Supplementary Information (ESI)

Liposomal nanohybrid cerasomes for mitochondria-targeted drug delivery

Yanfang Wang,[ab] Beibei Wang,[ab] Xiaojie Song,[ab] Hao Wu,[ab] Huihui Wang,[ab] Han Liao, [ab] Hujun Shen,[d] Guohui Li,[d] Xiaojun Ma [a] and Mingqian Tan [ac*]

[a.] *Division of Biotechnology, Dalian Institute of Chemical Physics, Chinese Academy of Sciences, Dalian 116023, China. E-mail: mqtan@dicp.ac.cn; Fax: +86-411-82463027; Tel: +86-411-82463027*

[b.] *University of the Chinese Academy of Sciences, Beijing 100049, China*

[c.] *State Key Laboratory of Molecular Reaction Dynamics, Dalian Institute of Chemical Physics, Chinese Academy of Sciences, Dalian 116023, China.*

[d.] *School of Food Science and Technology, Dalian Polytechnic University, Dalian 116034, China*

†Yanfang Wang and Beibei Wang contributed equally to this work.

Synthesis of cerasome-forming lipid

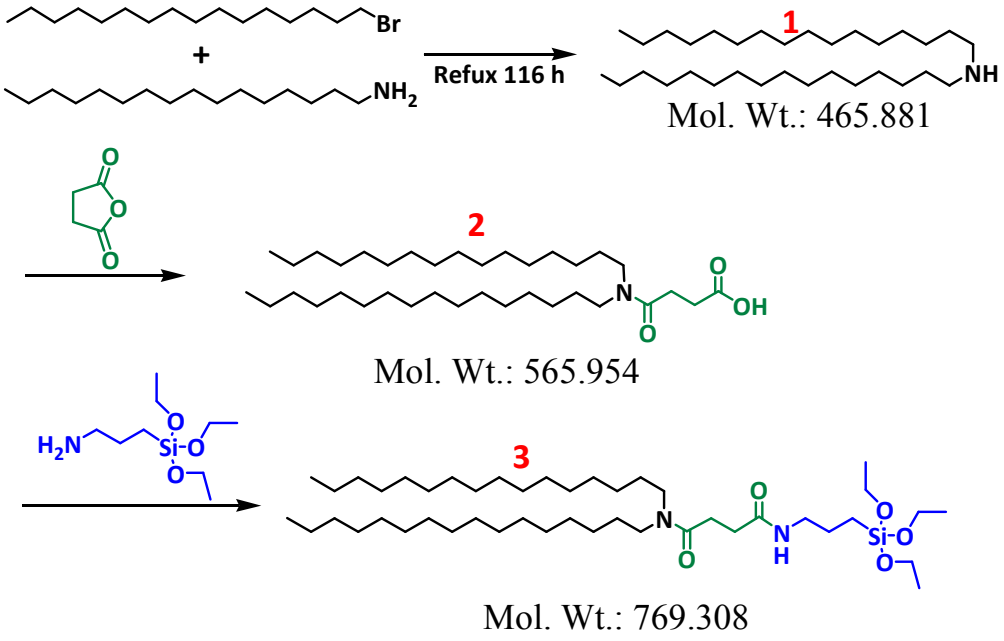

Scheme S1. The synthesis of cerasome-forming lipid

Synthesis of dihexadecylamine (compound 1)

A mixture of hexadecylamine (6.19 g, 25.6 mmol), bromohexadecane(6.50 g, 21.3 mmol) and 5.66g Na_2CO_3 was refluxed for 116 h in 50 mL anhydrous ethanol. The solvent was removed by evaporation and the residual solid was suspended in $CHCl_3$. The resulted product was washed with aqueous Na_2CO_3 and water (×2) followed by drying over by Na_2SO_4. The solvent was removed by evaporation and the residue was recrystallized from hexane for 3 times, and dried by vacuum desiccator to give dihexadecylamine as a white powder for compound 1 (5.85 g, 59% yield, Scheme S1). The final product was characterized by electrospray ionization (ESI) mass spectroscopy (MS) [(m/z, $[M+H]^+$):466.8(calculated), 466.5(observed), Fig. S1]

Synthesis of N, N'-dihexadecylsuccinamic acid (compound 2)

Dihexadecylamine (3.00 g, 6.44 mmol) and succinic anhydride (1.29 g, 12.9 mmol) were added to dry tetrahydrofuran (50 mL) and the solution was stirred for 24 h at room temperature. The solvent was evaporated in vacuo and the crude product was dissolved in 50 mL dichloromethane. The solution was

then washed with 10 % aqueous citric acid and saturated aqueous sodium chloride. After removing residual water using phase separation filter, the organic solvent was evaporated in vacuo. Subsequent recrystallization from acetonitrile gave a white solid for compound 2 (2.59 g, 71.2% yield, Scheme S1). ESI MS [(m/z, $[M+H]^+$): 566.9 (calculated), 566.4 (observed), Fig. S2]

Synthesis of N-[N-(3-Triethoxysilyl) propylsuccinamoyl] dihexadecylamine (compound 3)

DCC (1.01 g, 4.90 mmol) was added with stirring at 0°C to a solution of N,N'-Dihexadecylsuccinamic acid (2.40 g, 4.24 mmol) in 50 mL dry dichloromethane. After 15 min of stirring, 3-aminopropyltriethoxysilane (APS, 1.22 g, 5.51 mmol) was added to the solution and the mixture was stirred for 4 h at 0 °C and subsequently for a further 12 h at room temperature. Precipitates (N,N'-dicyclohexylurea) were removed by filtration. The resulted compound 3 was keep in dry dichloromethane for further use (3.00 g, 92% yield, Scheme S1). ESI MS [(m/z, $[M+H]^+$): 770.3 (calculated), 769.6 (observed), Fig. S3]

Synthesis of TPP (compound 4)

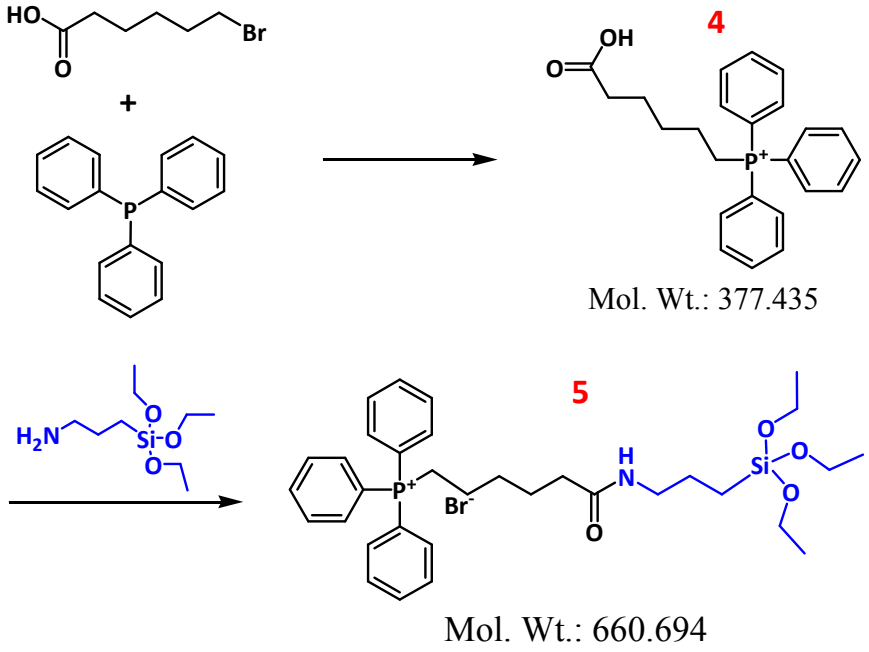

Scheme S2. Synthesis scheme of APS-TPP

A solution of 6-bromohexanoic acid (8.0 g, 41 mmol) and triphenylphosphine (11.3 g, 43mmol) in 50 mL CH_3CN was refluxed under dry N_2 for 16 h. Upon cooling to room temperature, the product begins to crystallize. The crystal product was filtered and washed with Et_2O (2×30mL) to afford a white powder as compound 4 [(5-carboxypenty1) triphenylphosphoniumbromide(TPP), 17.25 g, 92% yield, Scheme S2]. ESI MS [(m/z, $[M-Br]^+$):377.4(calculated), 377.9 (observed), Fig. S4]

Synthesis of TPP-APS (compound 5)

A solution of TPP (46 mg, 0.10 mM), EDC·HCl (21 mg, 0.11 mM) and NHS (14 mg, 0.12 mM) in DMF (5 mL) was stirred at room temperature for 20 minutes, followed by adding 21 μL (0.09 mM) APS. The mixture was stirred at room temperature for 24 h to prepare TPP-APS (54 mg, 90% yield, compound 5, Scheme S2). ESI MS [(m/z, $[M+H]^+$):580.8 (calculated), 580.8 (observed), Fig. S5]

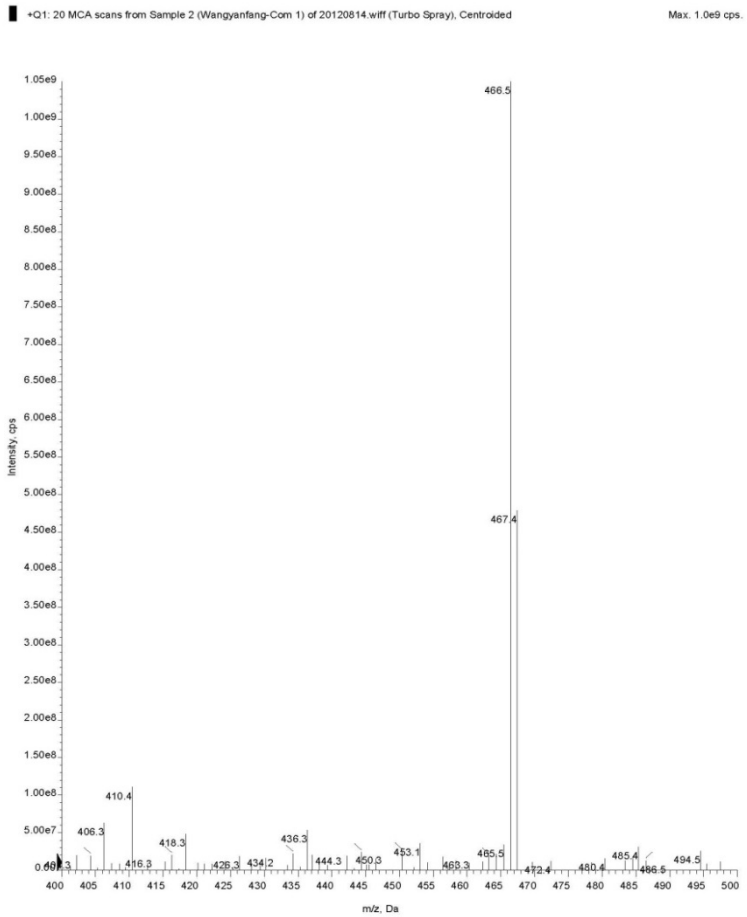

Fig. S1. The MS spectrum of dihexadecylamine (compound 1).

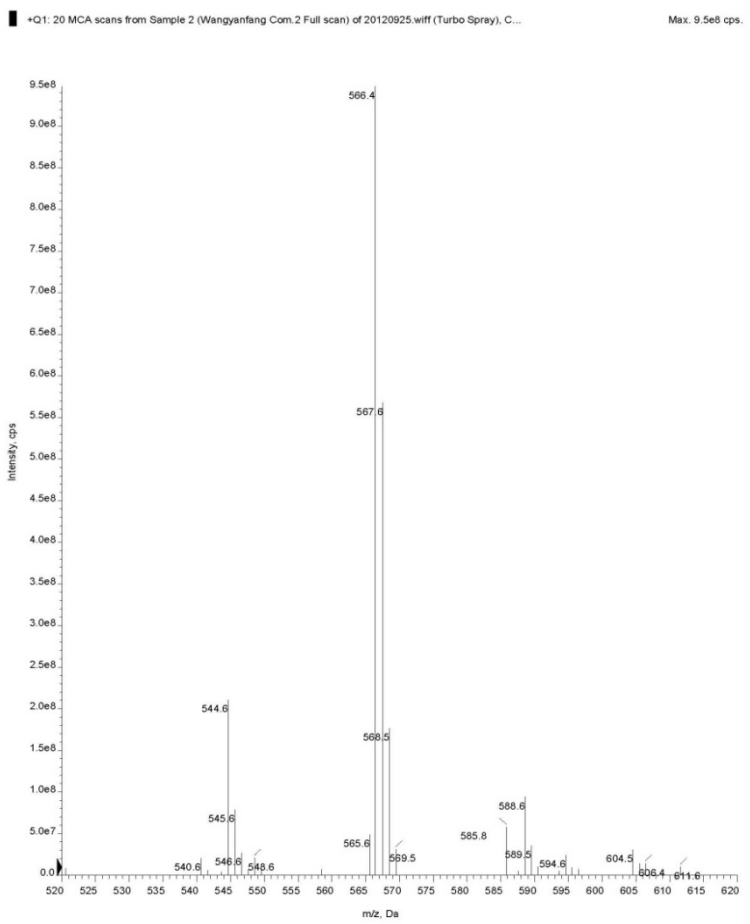

Fig. S2. MS spectrum of N,N'-dihexadecylsuccinamic acid (compound 2).

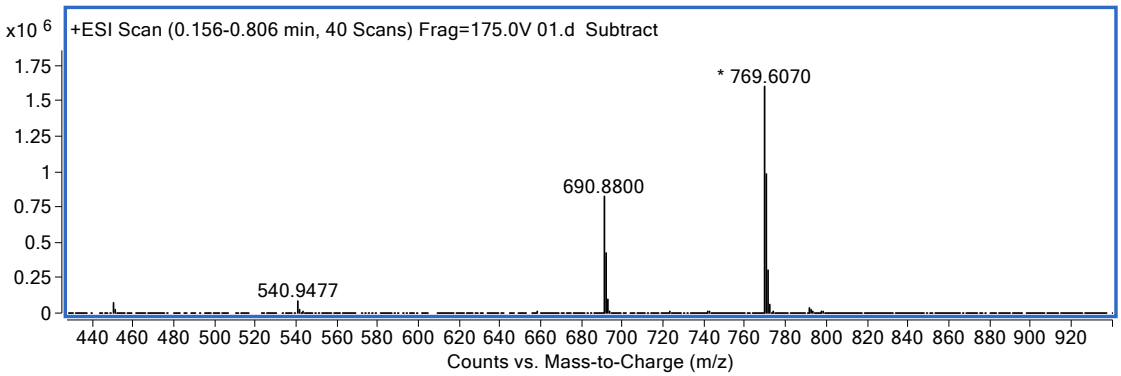

Fig. S3. MS spectrum of CFL

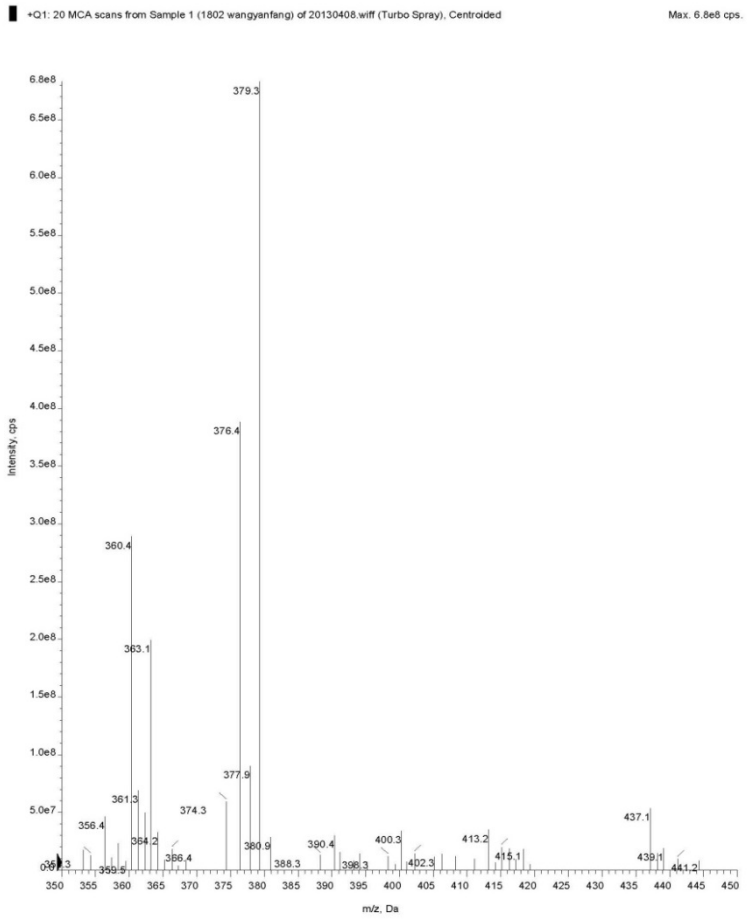

Fig. S4. MS spectrum of TPP-COOH.

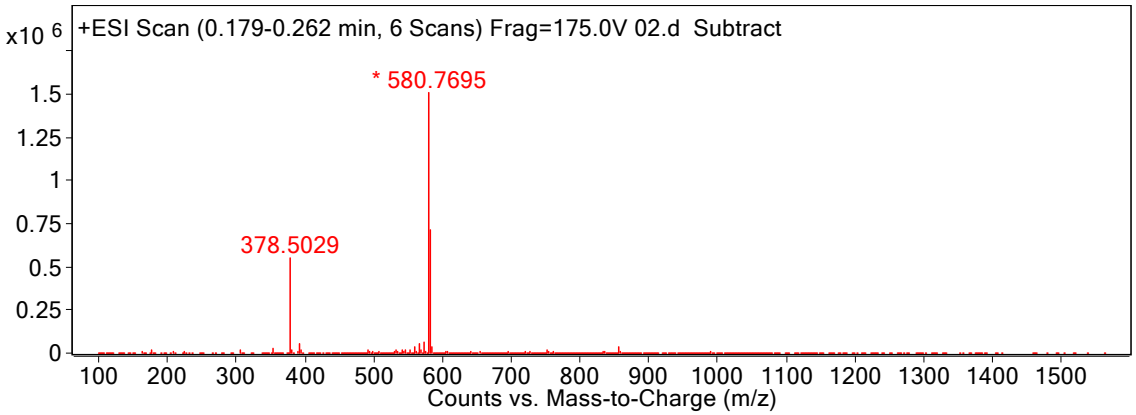

Fig. S5. MS spectrum of TPP-APS

DLS analysis of cerasomes (CER)

DLS data showed that the average size of pure CER, CER-DOX and TPP-CER-DOX nanoparticles was 213.6±7.2 nm, 226.5 ± 2.0 nm and 219.6 ± 10.6 nm, respectively (Fig. S6). The PDI of pure CER, CER-DOX and TPP-CER-DOX nanoparticles was 0.106, 0.155 and 0.096, respectively.

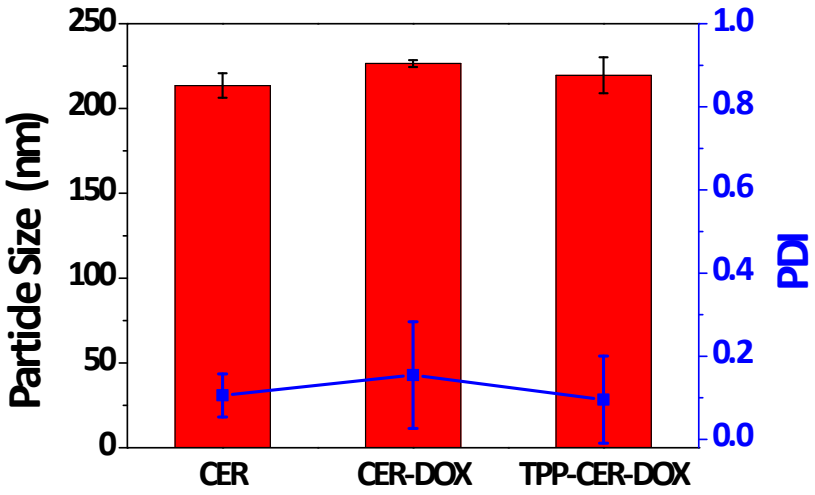

Fig. S6. The particle size and size distribution of pure CER, CER-DOX and TPP-CER-DOX nanoparticles

---

Time-storage stability

As a drug carrier, it is essential to retain the stability of structure during the storage and drug delivery process. To evaluate the time-storage stability, the cerasomes were kept at room temperature for 100 days. The DLS data showed that the initial hydrodynamic diameter was about 236.67 nm, while the diameter didn't change significantly in 100 days (Fig. S7). The stability of the hydrodynamic diameter suggested that the cerasomes were very suitable for long-time storage.

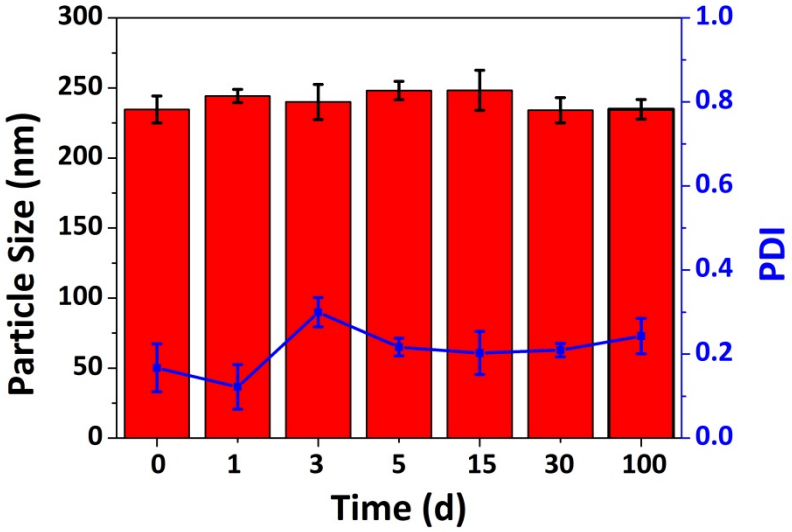

Fig. S7. Time-storage stability of cerasomes

Gay-Berne electric multipole (GBEMP) energy function

The effective energy function of GBEMP model is given by a sum of bonded and non-bonded energy terms:

$$U_{GBEMP} = U_{bond} + U_{angle} + U_{GB} + U_{EMP} \qquad (1)$$

where U_{bond}, and U_{angle} represent the bond stretching, angle bending and torsional potentials respectively. The non-bonded energy terms are described by U_{GB} and U_{EMP} that correspond to Gay-Berne anisotropic potential and electric multipole potential respectively.

In the GBEMP model, a fourth-order Taylor expansion of the Morse potential is used for the bond stretching energy term when the angle bending energy term adopts a sixth-order potential, and a three-term Fourier series expansion is employed to calculate torsional energies:

$$U_{bond} = K_b(b - b_0)^2\left[1 - 2.55(b - b_0) + \left(\frac{7}{12}\right)2.55(b - b_0)^2\right] \qquad (2)$$

$$U_{angle} = K_\theta(\theta - \theta_0)^2[1 - 0.014(\theta - \theta_0) + 5.6 \times 10^{-5}(\theta - \theta_0)^2 - 7.0 \times 10^{-7}(\theta - \theta_0)^3 + 2.2 \times 10^{-8}(\theta - \theta_0)^4 \quad (3)$$

$$U_{torsion} = \sum_n K_{n\phi}[1 + cos(n\phi \pm \delta)] \quad (4)$$

In this work, the bond stretching, angle bending and torsional potentials were parametrized by fitting to the atomistic profiles of the potentials of mean force (PMFs) constructed from atomistic conformations of silane.

The Gay-Berne anisotropic potential energy function U_{GB} is given as the form:

$$U_{GB}(\hat{u}_i,\hat{u}_j,\hat{r}_{ij}) = 4\varepsilon(\hat{u}_i,\hat{u}_j,\hat{r}_{ij})\left[\left(\frac{d_w\sigma_0}{r_{ij} - \sigma(\hat{u}_i,\hat{u}_j,\hat{r}_{ij}) + d_w\sigma_0}\right)^{12} - \left(\frac{d_w\sigma_0}{r_{ij} - \sigma(\hat{u}_i,\hat{u}_j,\hat{r}_{ij}) + d_w\sigma_0}\right)^{6}\right] \quad (5)$$

The range parameter $\sigma(\hat{u}_i,\hat{u}_j,\hat{r}_{ij})$ and the strength parameter $\varepsilon(\hat{u}_i,\hat{u}_j,\hat{r}_{ij})$ for pair-wise interactions are functions of the relative orientation of the Gay-Berne particles *i* and *j*. Each uniaxial molecule is associated with a set of Gay-Berne parameters that describe its shape (such as ellipsoid, sphere or disk) and the orientation of its principal axis in the inertial frame, defined according to its all-atom model. The term d_w is used to control the "softness" of the potential and σ_0 is defined as the square root of the sum of squared breadth of each particle.

The interaction energy between two electric multipole sites can be expressed as its polytensor form:

$$U_{EMP} = \sum_{ij} U_{ij} = \sum_{ij} V_i^T M_{ij} V_j \quad (6)$$

or its expanded form

$$U_{ij} = \begin{bmatrix} q_i \\ d_{ix} \\ d_{iy} \\ d_{iz} \\ Q_{ixx} \\ \vdots \end{bmatrix}^T \begin{bmatrix} 1 & \frac{\partial}{\partial x_j} & \frac{\partial}{\partial y_j} & \cdots \\ \frac{\partial}{\partial x_i} & \frac{\partial^2}{\partial x_i \partial x_j} & \frac{\partial^2}{\partial x_i \partial y_j} & \cdots \\ \frac{\partial}{\partial y_i} & \frac{\partial^2}{\partial y_i \partial x_j} & \frac{\partial^2}{\partial y_i \partial y_j} & \cdots \\ \vdots & \vdots & \vdots & \ddots \end{bmatrix} \left(\frac{1}{r_{ji}}\right) \begin{bmatrix} q_j \\ d_{jx} \\ d_{jy} \\ d_{jz} \\ Q_{jxx} \\ \vdots \end{bmatrix} \tag{7}$$

where q, d and Q are charge, dipole and quadrupole moments respectively. When the EMP sites are determined in a rigid body, it should be straightforward to obtain the EMP parameters for the CG particle through the electric multipole expansion at the specific locations based on an atomistic model.

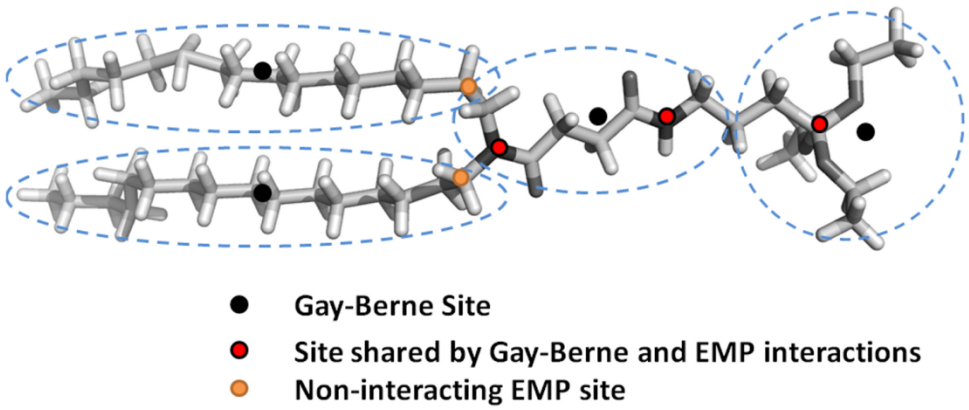

Fig. S8. GBEMP mapping for CFL. Each rigid body, being enclosed by a dash line, is composed of a Gay-Berne interacting site and one or more electric multipole (EMP) sites. Gay-Berne interacting sites are indicated black filled circles while the interacting EMP sites and non-interaction EMP sites are indicated by red and orange filled circles respectively. Red filled circles represent the sites shared by Gay-Berne and EMP interactions.

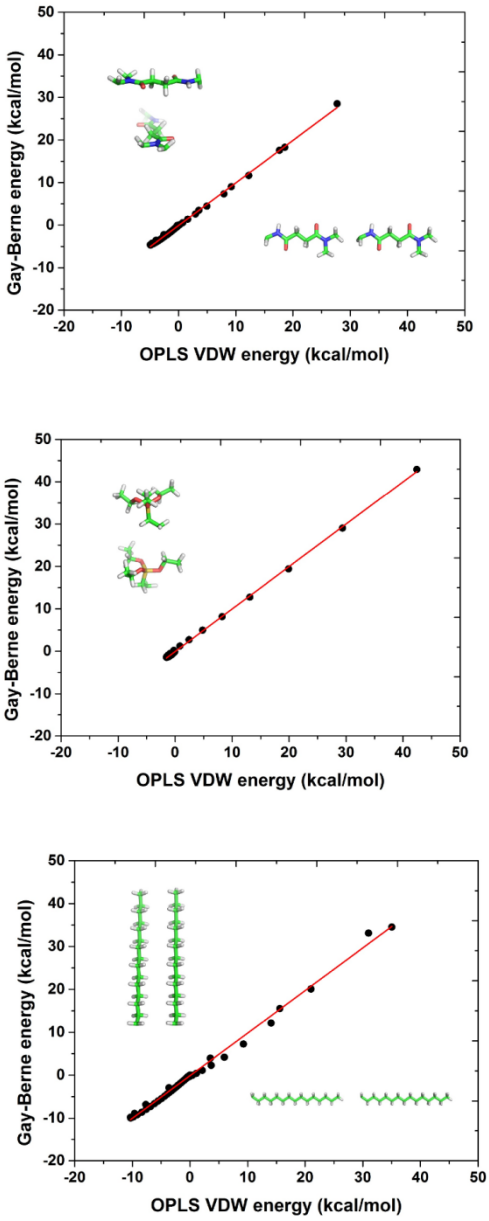

Fig. S9. Correlations between the GBEMP and atomistic (OPLS) results in the calculations of van der Waals (VDW) interactions between the homodimers respectively. In each figure, insets display the homodimers adopting different orientations.

GBEMP force field for CFL

###################### Mu   Nu

munudw 2.0 1.0

###

Tail rgbtype 12

###

crslm 12   "Tail21" 211.0 92.0 1070.0 1070.0

gblst 12   122

mplst 12   121

GB Amide site:Center of Mass

gbcrs   122 14.171 2.768   0.389 0.067 1.264 10.436

gbsite 122 0.000 0.000 0.000   1.0   0.0   0.0

EMP site (C)

charge 121   0.000   1.000

mpsite 121   8.914423   0.046827   0.197846

###

Tail rgbtype 13

###

crslm 13   "Tail22" 211.0 92.0 1070.0 1070.0

gblst 13   132

mplst 13   131

GB Amide site:Center of Mass

gbcrs 132 15.171 2.468 0.389 0.067 1.264 10.436

gbsite 132 0.000 0.000 0.000 1.0 0.0 0.0

EMP site (C)

charge 131 0.000 1.000

mpsite 131 -8.761357 0.417558 -0.365652

##

Silipid (S51) rgbtype is 51

##

Mass Ix Iy Iz

crslm 51 "S51" 155.000 154.408 585.922 627.056

gblst 51 512

mplst 51 511 513

################ GB Center of mass

gbcrs 512 7.500 3.426 2.868 0.149 1.057 3.190

gbsite 512 0.000 0.000 0.000 1.0 0.0 0.0

################ EMP site@Center

charge 511 -0.000 1.315

dipole 511 0.039 -0.207 0.278

mpsite 511 1.671428 1.668688 -0.019266

################ EMP site@Center

charge 513 -0.000 1.315

dipole 513 -0.371 0.413 -0.164

mpsite 513 -2.272214 -1.361135 -0.003862

##

Silipid (S52) rgbtype is 52

##

Mass Ix Iy Iz

crslm 52 "S52" 191.000 500.0 500.0 500.0 sphere

gblst 52 522

mplst 52 521

################ GB Center of mass

gbcrs 522 4.717 4.717 1.427 1.000 1.057 1.000

gbsite 522 0.000 0.000 0.000 0.0 0.0 1.0

################ EMP site@Center

charge 521 0.000 1.315

dipole 521 0.268 0.275 -0.526

mpsite 521 0.000 0.000 0.000

################################## Bond terms #####################################

##Silipid

crsbond 131 511 250.0 3.200

crsbond 511 121 250.0 4.400

crsbond 513 521 150.0 7.300

################################## Angle terms ######################################

##Silipid

crsangle 132 131 511 100.0 160.0

crsangle 131 511 512 100.0 120.0

crsangle 512 513 521 100.0 120.0

crsangle 512 511 121 100.0 70.0

crsangle 511 121 122 100.0 120.0

Drug loading capacity (DLC) and encapsulation efficiency (EE)

The drug loading capacity (DLC) and encapsulation efficiency (EE) of drug-loaded nanoparticles were determined by microfiltration. It was found that the free DOX and curcumin can freely through the springe filter (Tianjing Jingteng Experiment Equipment Co., Ltd. China), which was made of polyethersulfone microfiltration membrane, while CER nanoparticles can't through the microfiltration (Fig. S10). Briefly, 5 mL drug-loaded CER was placed in a syringe, then the solution was pushed through the PES microfiltration. The absorbance of the drug-loaded CER solution and filtrate was measured by ultraviolet spectrophotometer. Using the standard calibration curve, the amount of drug encapsulated in CER nanoparticles was calculated.

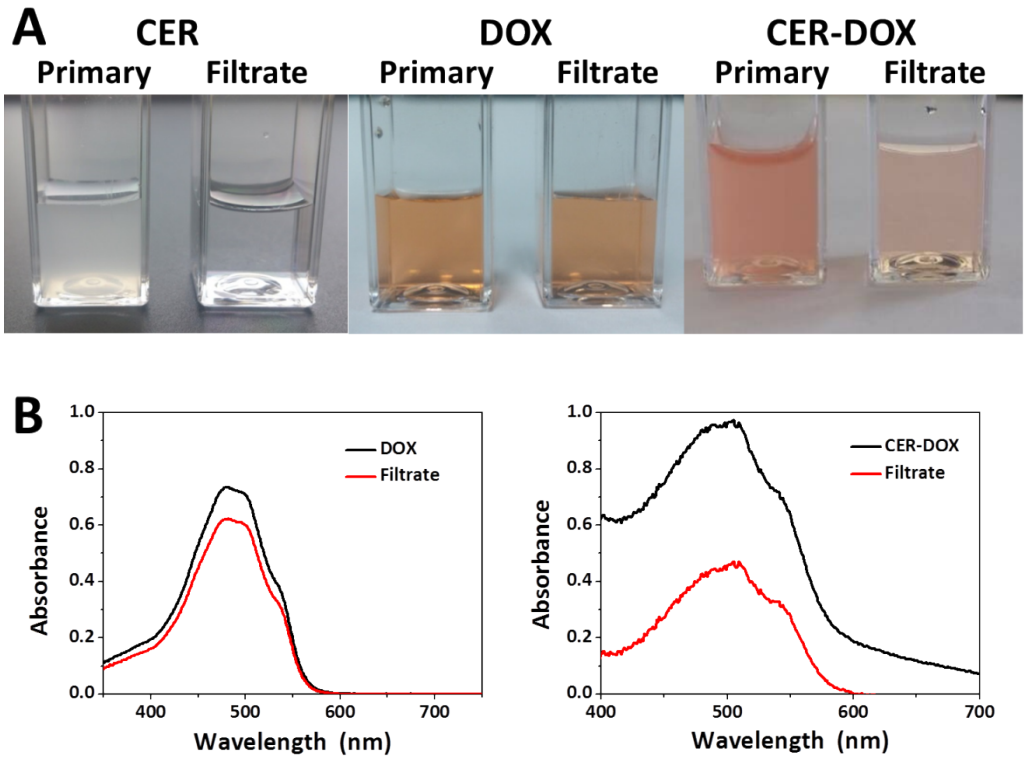

Fig. S10. Analysis of the drug loading capacity. (A) Cerasomes, DOX and CER-DOX solutions before and after the filtration by the syringe filter. DOX can freely pass through the syringe filter while CER cerasomes can't pass through the microfiltration. (B)The absorbance of the drug-loaded CER solution and filtrate was measured by ultraviolet spectrophotometer.

Fluorescence Intensity of CER-DOX

The concentration of DOX was determined by ultraviolet spectrophotometer at 488 nm, while the loading of DOX was determined by fluorospectrophotometer at an excitation wavelength of 470 nm and the spectra was collected at the range of 515 to 750 nm. The fluorescence intensity of DOX (Fig. S11) encapsulated in cerasome was of 32.68% compare to intensity of equal concentration of free DOX.

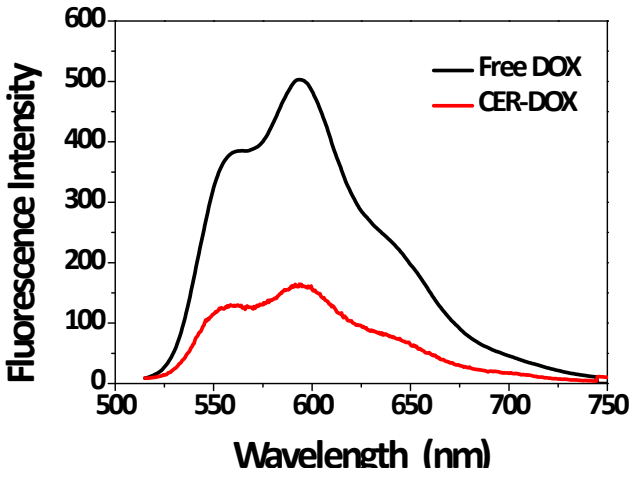

Fig. S11. Fluorescence intensity of equal concentration of DOX in free DOX solution and CER-DOX. The result shows that the fluorescence intensity reduced 2/3 after the DOX being encapsulated by cerasome.

Table S1. Zeta-potential of CER, TPP-CER and CER-DOX

	CER	TPP-CER	CER-DOX
Zeta potential (mV)	–18.61±6.41	+15.37±0.68	–13.49±2.17